Isothermal Crystallization of Poly(ethylene-*co*-glycidyl methacrylate)/Clay Nanocomposites

Jiann-Wen Huang,[1] Chiun-Chia Kang,[2] Tse-Hsin Chen[3]

[1]*Department of Styling and Cosmetology, Tainan Women's College of Arts and Technology, 529 Chung Cheng Road, Yung Kang City, 710, Taiwan, Republic of China*
[2]*R&D Center, Taroko International Company, Limited, 473 Jong Shan South Road, Yung Kang City 710, Taiwan*
[3]*Department of Chemistry, National Cheng Kung University, No. 1, Ta-Hsueh Road, Tainan 701, Taiwan*

Received 19 February 2004; accepted 14 June 2004
DOI 10.1002/app.21120
Published online in Wiley InterScience (www.interscience.wiley.com).

ABSTRACT: Poly(ethylene-*co*-glycidyl methacrylate) (PEGMA)/clay nanocomposites with clay concentrations of 1, 3, or 5 wt % were prepared via y melt blending in a twin-screw extruder. Wide-angle X-ray diffraction showed that the clay layers were intercalated by PEGMA. Differential scanning calorimetry was used to analyze the isothermal crystallization, and the equilibrium melting temperature was determined with the Hoffman–Weeks method. The Avrami, Tobin, Malkin, and Urbanovici–Segal models were applied to describe the kinetics of crystallization from the melt state under isothermal conditions. The crystallization kinetics showed that the addition of clay facilitated the crystallization of PEGMA, with the clay functioning as a heterophase nucleating agent; at higher concentrations, however, the physical hindrance of the clay layers to the motion of PEGMA chains retarded the crystallization process. © 2005 Wiley Periodicals, Inc. J Appl Polym Sci 97: 1051–1064, 2005

Key words: clay; crystallization; kinetics (polym.); nanocomposites

INTRODUCTION

Recent interest in polymer/clay nanocomposites stems from the dramatic improvements in their thermal and mechanical properties achievable by the addition of just a small fraction of clay to a polymer matrix. These composites exhibit improved modulus, a lower thermal expansion coefficient and gas permeability, higher swelling resistance, and enhanced ionic conductivity in comparison with pristine polymers because of the nanoscale structure of the hybrids and the synergism between the polymer and the silicate.[1–10]

The intercalation of layered silicates has proven to be a versatile approach for the preparation of nanocomposites. The preparation involves the intercalation of a suitable monomer and the exfoliation of the layered galleries into their nanoscale elements by subsequent polymerization. However, this method requires a proper monomer or solvent as a medium, and such a requirement puts a strong restraint on the selection of polymers used for the composites. Thus far, only a few polar polymers, such as epoxide polymer,[11,12] poly(ethylene oxide),[13] and polystyrene,[14] have been successfully prepared with intercalation. These polar polymers have been successful because they can be intercalated between smectic layers of the clay, from which the nanocomposites are derived.[15–18]

Several researchers have successfully prepared nanocomposites by direct melt blending in a twin-screw extruder with maleic anhydride grafted polypropylene[19–24]and polyethylene.[25] In this study, the nanocomposites were prepared through the blending, in a twin-screw extruder, of poly(ethylene-*co*-glycidyl methacrylate) (PEGMA) and clay. PEGMA contained epoxy groups that could intercalate between smectite layers. Models proposed by Avrami, Tobin, Malkin, and Urbanovici and Segal were used to analyze the isothermal crystallization kinetics of the nanocomposites.

EXPERIMENTAL

Materials

Commercial-grade PEGMA (CG5004) was supplied by Sumitomo Chemical Co, Ltd. (Tokyo, Japan); it contained 81 wt % ethylene and 19 wt % glycidyl methacrylate. Modified montmorillonite clay (KH-γc) was purchased from Vulchem (Taipei, Taiwan). Both materials were used as received without purification:

Correspondence to: J.-W. Huang (jw.huang@msa.hinet.net).

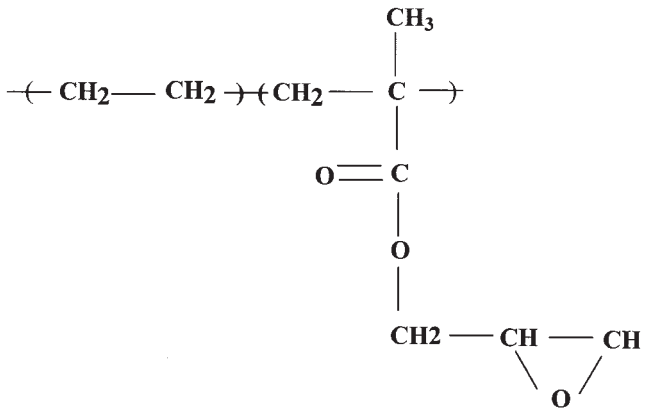

81 wt% 19 wt%

Sample preparation

All the materials were dried at room temperature in a vacuum oven for 6 h before compounding. PEGMA and 20 wt % clay were compounded with a twin-screw extruder (CM-MTE, Continent Machinery Co., Tainan, Taiwan) at 180°C and 300 rpm to make a master batch. The master batch was then mixed with PEGMA and recompounded at 160°C and 300 rpm to prepare 1 (PEGMA/clay1), 3 (PEGMA/clay3), and 5 wt % (PEGMA/clay5) nanocomposites.

Characterization

Wide-angle X-ray diffraction (WAXD)

X-ray diffraction (XRD) was performed with a Shimadzu (Kyoto, Japan) XD-D1 with Cu Kα radiation (wavelength = 1.54051 Å). The generator was operated at 40 kV and 20 mA. The samples were placed inside an aluminum sample holder at room temperature and were scanned at diffraction angles ranging from 2 to 10° at a scanning rate of 1°/min.

Isothermal crystallization

The crystallization behaviors of the PEGMA/clay nanocomposites were investigated with a PerkinElmer (Wellesley, MA) DSC-1 differential scanning calorimeter. The differential scanning calorimeter was calibrated with indium with sample weights of 8–10 mg. All operations were carried out in a nitrogen atmosphere. Before the data gathering, the samples were heated to 120°C and held in the molten state for 5 min to eliminate the influence of the thermal history. The sample melts were then quenched at a rate of 100°C/min to reach the specific temperature and were kept at that temperature for 1 h. When the isothermal crystallization was completed, the samples were heated to 120°C at a rate of 10°C/min to measure the melting temperatures (T_m's).

Polarized optical microscopy

The sample morphologies were observed under polarized light with a Nikon (Tokyo, Japan) polarized optical microscope. The samples, on glass slides covered with slips, were heated to 120°C to melt, were held for 5 min at that temperature, and then were set to the

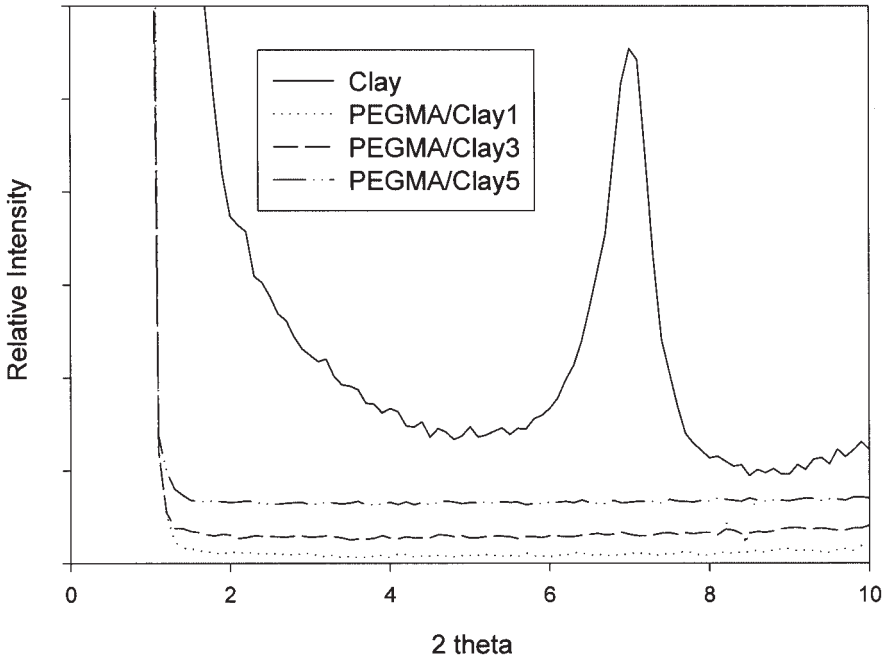

Figure 1 WAXD patterns of PEGMA and PEGMA/clay nanocomposites.

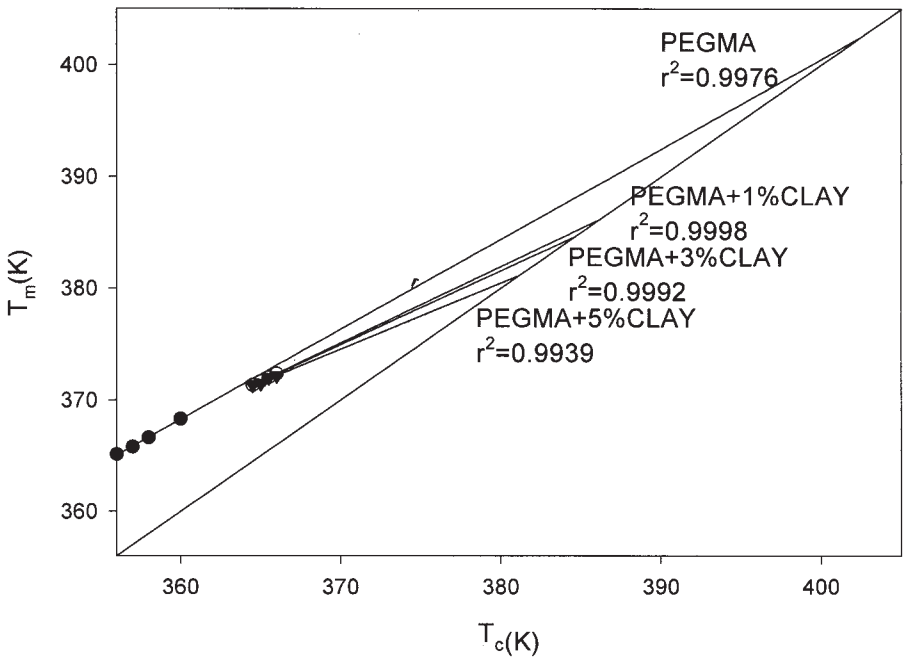

Figure 2 Hoffman–Weeks plot for PEGMA and PEGMA/clay nanocomposites.

crystallization temperature (T_c) for complete crystallization.

RESULTS AND DISCUSSION

WAXD analysis

XRD is an effective technique for detecting the existence of stacking layers in a polymer/clay system. The characteristic diffraction peak corresponding to the stacking of the clay layers (001 plane) can be observed at low angles (i.e., $2\theta < 10°$). The peak shifts to lower angles when intercalation occurs, and the peak disappears if some exfoliation has occurred.

Figure 1 shows XRD patterns for clay and PEGMA/clay nanocomposites. The interlamellar spacing for the (001) plane of the neat clay is 12.15 Å ($2\theta = 7.27°$). However, there are no diffraction peaks for PEGMA/clay1, PEGMA/clay3, and PEGMA/clay5, and this suggests that there are no stacking layers present in those PEGMA/clay blends and that layers have been homogeneously dispersed. Molecular chains of PEGMA could have been intercalated into the clay interlayer by the interactions between the epoxy groups and the clay surface.

Equilibrium melting temperature (T_m^0)

The Hoffman–Weeks relation[26] has been extensively accepted for estimating T_m^0:

$$T'_m = T_m^0\left(1 - \frac{1}{\gamma}\right) + \frac{T_c}{\gamma} \quad (1)$$

The constant γ is equal to l/l^*, l and l^* being the lamellar thickness at the time of melting and the thickness of the critical nucleus at T_c, respectively.[27] T'_m is the observed melting temperature. Figure 2 shows plots of T_m versus T_c for PEGMA and PEGMA/clay nanocomposites. A good linear correlation between T_m and T_c can be observed. According to eq. (1), T_m^0 could be determined by the extrapolation of T_m versus T_c to $T_m = T_c$. The results are shown in Table I. The T_m^0 value of PEGMA was strongly reduced by the blending with clay, and this indicated that the crystals formed in the blends were smaller and less perfect than the crystals of neat PEGMA, probably because of the interaction of the epoxy group of PEGMA and the clay surface. Kuo et al.[28] reported that the ion–ion interactions in the clay nanocomposites could reduce to T_m^0.

Crystallization kinetics

Avrami analysis

Figure 3 shows the relative crystallinity [$X(t)$] at different T_c's. $X(t)$ is defined as the ratio of crystallinity

TABLE I
T_m^0 of PEGMA and PEGME/Clay Nanocomposites

Sample	T_m^0 (K)
PEGMA	402
PEGMA and 1% clay	386
PEGMA and 3% clay	384
PEGMA and 5% clay	381

developed at crystallization time t to that developed at time $t \rightarrow \infty$. The Avrami equation[29–35] can be used to analyze the isothermal melt crystallization of PEGMA and PEGMA/clay nanocomposites:

$$X(t) = 1 - \exp[-(K_a t)^{n_a}] \quad (2)$$

where K_a is the Avrami crystallization rate constant and n_a is the Avrami exponent. $X(t)$ can be calculated as the ratio of the area of the exothermic peak at time t to the total measured area of crystallization. The values of K_a and n_a were determined through the fitting of experimental data

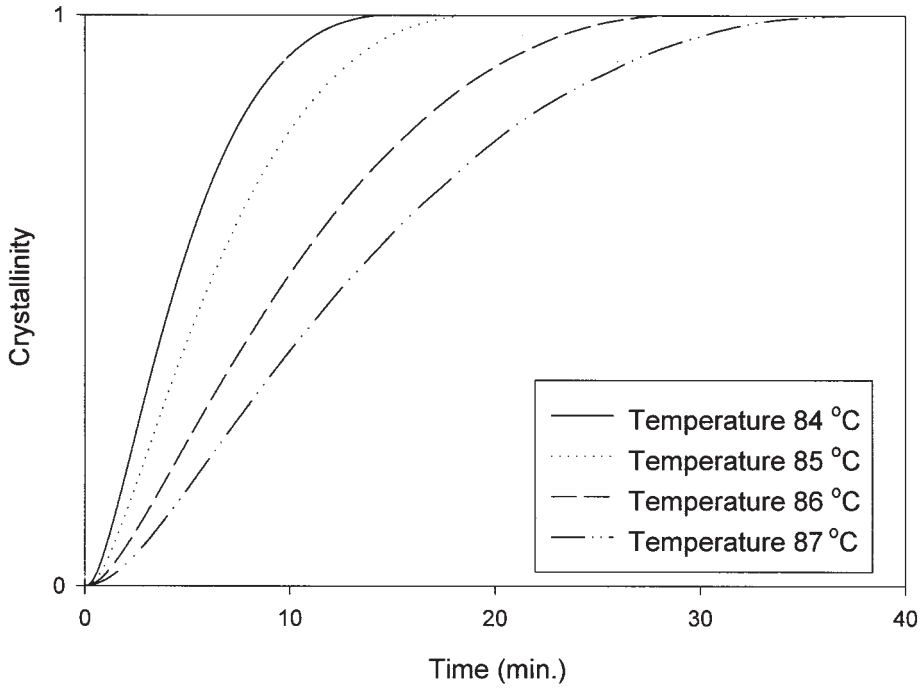

(A)

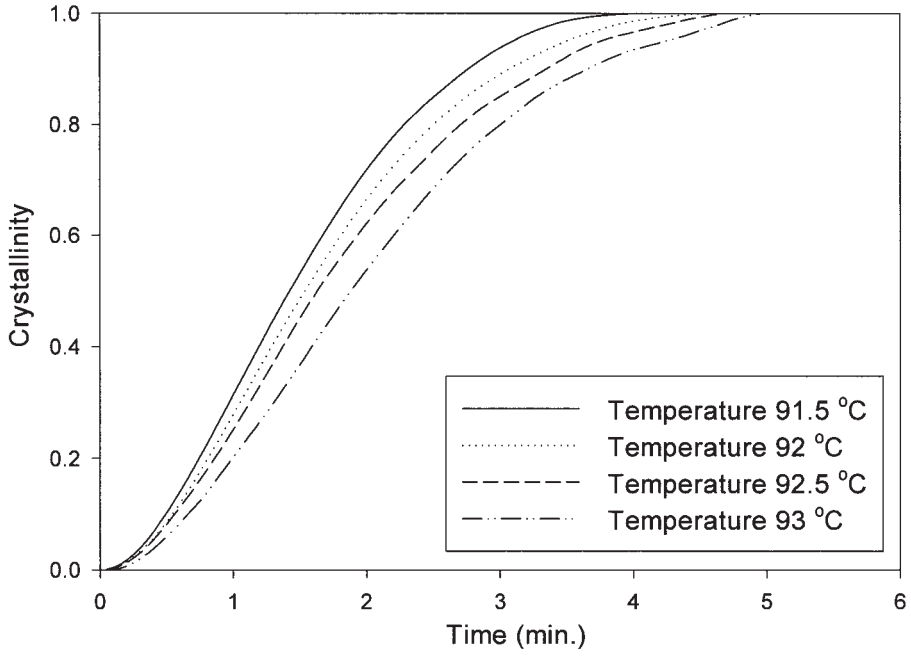

(B)

Figure 3 $X(t)$ as a function of time: (A) PEGMA, (B) PEGMA/clay1, (C) PEGMA/clay3, and (D) PEGMA/clay5.

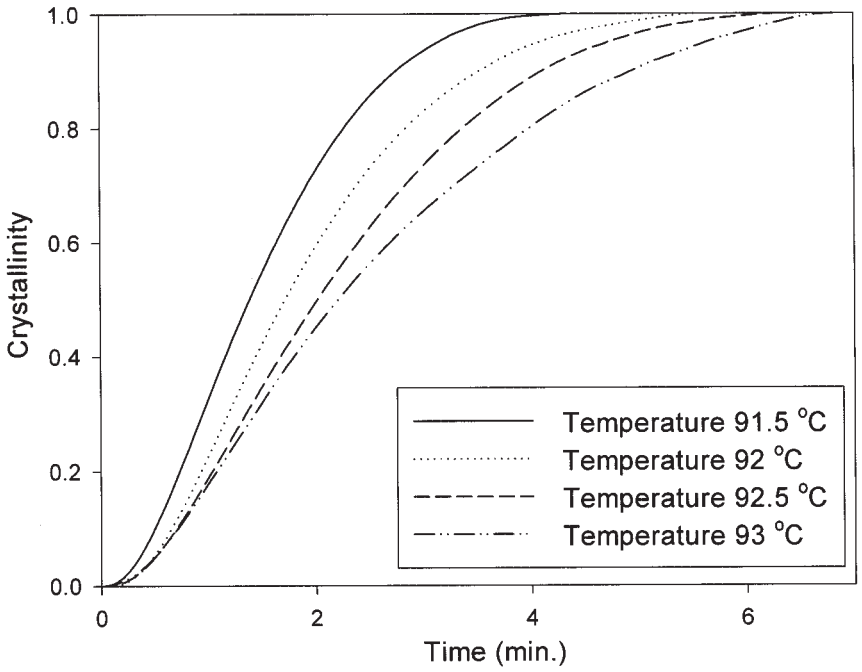

(C)

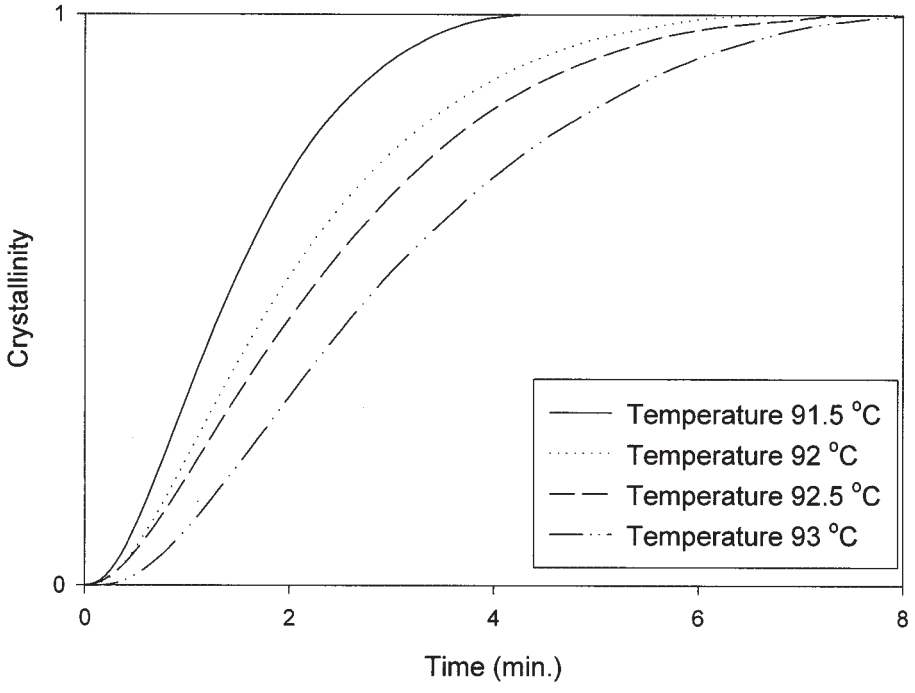

(D)

Figure 3 (*Continued from the previous page*)

of $X(t)$ to eq. (2), and the results are shown in Table II.

The Avrami expression is usually written as[31,32]

$$X(t) = 1 - \exp(-k_a^* t^{n_a^*}) \quad (3)$$

or

$$\ln\{-ln[1 - X(t)]\} = \ln k_a^* + n_a^* \ln t \quad (4)$$

The values of k_a^* and n_a^* can be determined from the slope and intercept with the y axis by the plotting of $\ln\{-\ln[1 - X(t)]\}$ versus $\ln(t)$, as shown in Figure 4, and the results are shown in Table II. Each curve shows an initial linear portion and then subsequently

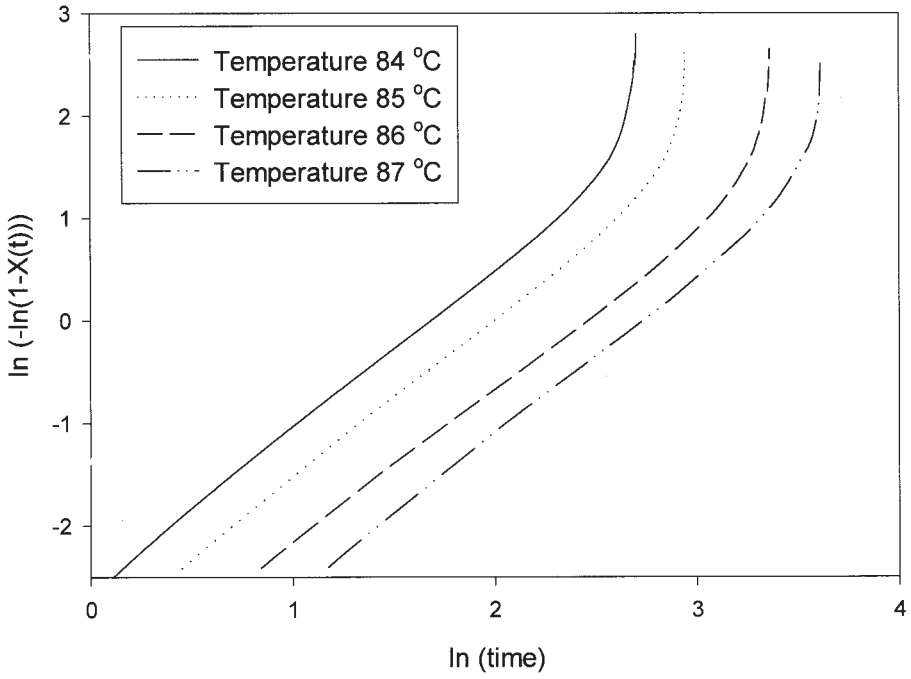

(A)

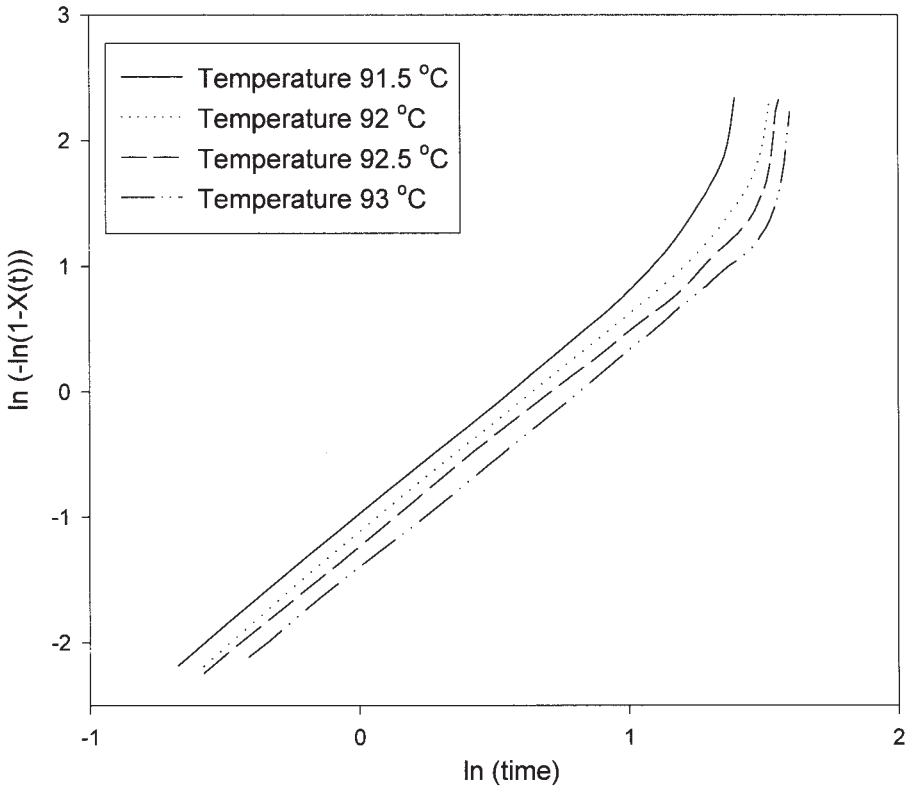

(B)

Figure 4 Avrami analysis from eq. (4) for PEGMA and PEGMA/clay nanocomposites: (A) PEGMA, (B) PEGMA/clay1, (C) PEGMA/clay3, and (D) PEGMA/clay5.

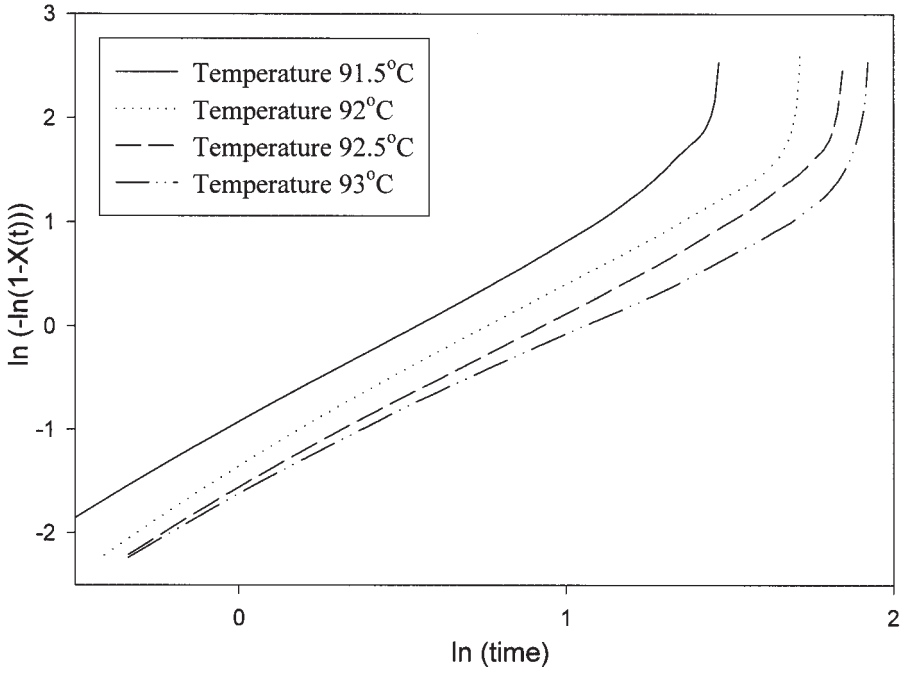

(C)

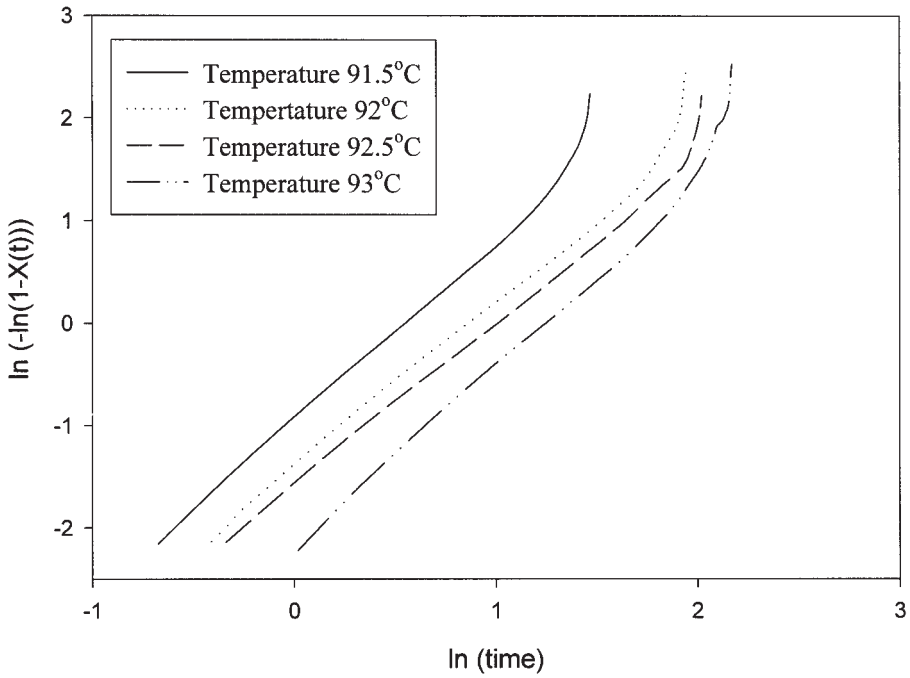

(D)

Figure 4 (*Continued from the previous page*)

tends to level off. This leveling off is thought to be due to the effect of the secondary crystallization, which is caused by spherulite impingement in the later stage of crystallization.[36–38] The Avrami rate constant k_a^* is a function of both the temperature and n_a (i.e., $k_a^* = K_a^n$). The use of K_a is preferable because k_a^* is independent of the Avrami exponent.[39–41]

The crystallization half-time ($t_{1/2}$) is defined as the time at which the extent of crystallization is 50%. The crystallization rate constant can be derived from eq. (2) and expressed as follows:[36,40]

$$K_a' = (\ln 2)^{\frac{1}{n_a}} t_{1/2}^{-1} \tag{5}$$

TABLE II
Avrami Kinetic Parameters and $t_{1/2}$

Sample	T_c (°C)	n_a	K_a (min^{-1})	R^2	n_a*	k_a* (min^{-n})	$t_{1/2}$ (min)	K_a' (min^{-n})
PEGMA	84	1.55	0.1886	0.9996	1.53	0.0761	4.22	0.1871
	85	1.56	0.1373	0.9993	1.52	0.0485	5.76	0.1373
	86	1.55	0.0869	0.9986	1.46	0.0275	9.13	0.0865
	87	1.58	0.0622	0.9987	1.50	0.0165	12.01	0.0660
PEGMA and 1% clay	91.5	1.81	0.5758	0.9994	1.76	0.3748	1.42	0.5751
	92	1.86	0.5393	0.9997	1.84	0.3193	1.54	0.5332
	92.5	1.74	0.4910	0.9996	1.73	0.2923	1.63	0.4970
	93	1.76	0.4451	0.9997	1.73	0.2449	1.83	0.4437
PEGMA and 3% clay	91.5	1.77	0.5641	0.9997	1.76	0.3667	1.45	0.5607
	92	1.74	0.4652	0.9995	1.80	0.2542	1.73	0.4682
	92.5	1.70	0.3975	0.9996	1.69	0.2097	2.02	0.3990
	93	1.52	0.3486	0.9989	1.65	0.1828	2.24	0.3508
PEGMA and 5% clay	91.5	1.71	0.5780	0.9996	1.71	0.3618	1.46	0.5528
	92	1.56	0.4192	0.9995	1.60	0.2510	1.86	0.4251
	92.5	1.56	0.3676	0.9997	1.55	0.2005	2.14	0.3694
	93	1.73	0.2886	0.9993	1.68	0.1716	2.32	0.3487

There is good agreement between K_a' and K_a, as shown in Table II.

Table II shows Avrami kinetic parameters and $t_{1/2}$ values at different T_c's. Crystallization rate constants, K_a, k_a^*, and K_a' for neat PEGMA and PEGMA/clay samples decreased with increasing T_c. A higher T_c means a lower degree of supercooling and greater difficulty for the formation of nuclei. The crystallization rates of PEGMA/clay composites were faster than those of neat PEGMA, and this could be ascribed to the effects of clay as an efficient nucleating agent for facilitating PEGMA crystallization. The crystallization rate of PEGMA in PEGMA/clay3 and PEGMA/clay5 was slower than that in PEGMA/clay1, and this suggested that a larger amount of clay tended to retard the crystallization process. The overall isothermal crystallization rate was governed by nucleation and diffusion.[43] When the content of clay was high, its function as a nucleating agent was overwhelmed by the physical hindrance to the diffusion, and thus the overall crystallization rate was reduced. Similar effects have been studied in other nanocomposite system.[44–46]

The n_a and n_a^* values varied from 1.46 to 1.58 for neat PEGMA and from 1.55 to1.86 for all three PEGMA/clay systems. This indicated that the addition of clay apparently did not change the crystallization mechanism of PEGMA.

To test the efficiency of the models in describing the isothermal crystallization kinetics, we reconstructed $X(t)$ as a function of time for each model. The reconstruction was carried out for all clay compositions, but only PEGMA/clay3, crystallized at 92°C, is presented to simplify the presentation. A comparison of the various models (Fig. 5) indicated that the Avrami model provided a good fit to the experimental data.

Tobin analysis

The Avrami analysis is only appropriate for early stages of crystallization. To improve the Avrami equation for the later stages of crystallization, Tobin[47–49] proposed a theory of phase transformation kinetics with growth site impingement:

$$X(t) = \frac{(K_t t)^{n_t}}{1 + (K_t t)^{n_t}} \tag{6}$$

where K_t is the Tobin rate constant and n_t is the Tobin exponent. n_t does not need to be a integer and is mainly governed by different types of nucleation and growth. The Tobin crystallization parameters (K_t and n_t) were determined by the fitting of the $X(t)$ data obtained for each T_c to eq. (6), and the results are shown in Table III.

Equation (6) can also be written in a simplified form:

$$X(t) = \frac{k_t^* t^{n_t^*}}{1 + k_t^* t^{n_t^*}} \tag{7}$$

or

$$\ln \frac{X(t)}{1 - X(t)} = \ln k_t^* + n_t^* \ln t \tag{8}$$

Tobin rate constant k_t^* is written in a composite form (i.e., $k_t^* = K_t^{n_t}$) and is a function of the temperature and n_t. The use of K_t is preferable because K_t is independent of n_t.[39–41,48] The crystallization parameters ($k_t^*$and n_t^*) were found by the drawing of a least-square line [from $X(t) = 0.1$ to $X(t) = 0.8$] to fit the double logarithmic plot of $\ln\{X(t)/[1 - X(t)]\}$ versus $\ln(t)$. k_t^* was taken as the antilogarithmic value of the y intercept,

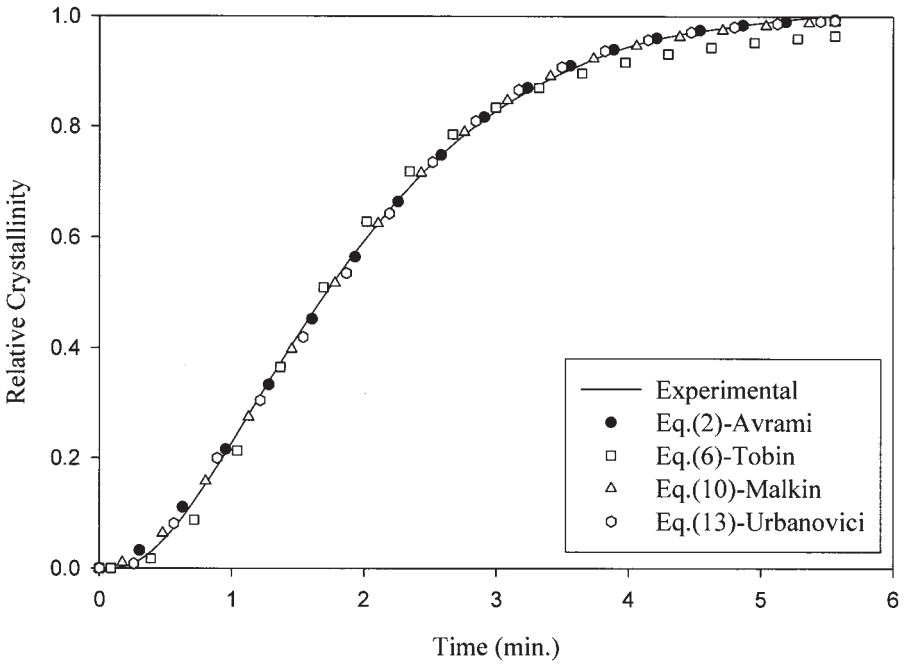

Figure 5 Experimental data for PEGMA/clay3 isothermal crystallization at 92°C fitted to the Avrami, Tobin, Malkin, and Urbanovici–Segal models.

and n_t^* was the slope. The results are shown in Figure 6 and Table III. The simplified form of eq. (7) provided a good fit to the experimental data for a major portion of $X(t)$, but eq. (7) always gave $X(t)$ values lower than the experimental data. The underprediction has been attributed to an overemphasis of the impingement effect and the mathematical simplification of eq. (7).[50,51] K_t' can be estimated directly from the reciprocal of $t_{1/2}$ as follows:

$$K_t' = \frac{1}{t_{1/2}} \tag{9}$$

The estimated K_t' values are also listed in Table III for comparison, and a good agreement can be observed between K_t' and K_t.

n_a is always lower than n_t at an arbitrary crystallization. Taking the average of the difference between the two values, we find $n_t \cong n_a + 1$, which agrees with the observations of others.[52–54] According to Figure 5, the Tobin model appears to underestimate $X(t)$ at the early and later stages and overestimate it at the middle stage. Regression coefficient (R^2) analysis also indicated that the Tobin model was not satisfactory in describing the experimental data.

TABLE III
Tobin Kinetic Parameters

Sample	T_c (°C)	n_t	K_t (min^{-1})	R^2	n_t*	k_t* (min^{-n})	K_t' (min^{-n})
PEGMA	84	2.48	0.2469	0.9898	2.03	0.0582	0.2369
	85	2.47	0.1841	0.9884	2.01	0.0319	0.1736
	86	2.42	0.1152	0.9855	1.94	0.0152	0.1095
	87	2.47	0.0874	0.9863	1.99	0.0078	0.0832
PEGMA and 1% clay	91.5	2.84	0.7343	0.9897	2.32	0.5356	0.7042
	92	2.96	0.6832	0.9921	2.34	0.3753	0.6493
	92.5	2.79	0.6318	0.9912	2.28	0.3511	0.6134
	93	2.74	0.5703	0.9910	2.27	0.2788	0.5464
PEGMA and 3% clay	91.5	2.80	0.7289	0.9916	2.34	0.5156	0.6896
	92	2.77	0.5985	0.9947	2.40	0.2892	0.5780
	92.5	2.69	0.5146	0.9913	2.25	0.2332	0.4955
	93	2.34	0.4644	0.9902	2.03	0.2096	0.4464
PEGMA and 5% clay	91.5	2.70	0.7177	0.9921	2.23	0.5028	0.6849
	92	2.51	0.5541	0.9931	2.15	0.2799	0.5376
	92.5	2.49	0.4860	0.9911	2.07	0.2238	0.4679
	93	2.73	0.3727	0.9916	2.30	0.1019	0.4310

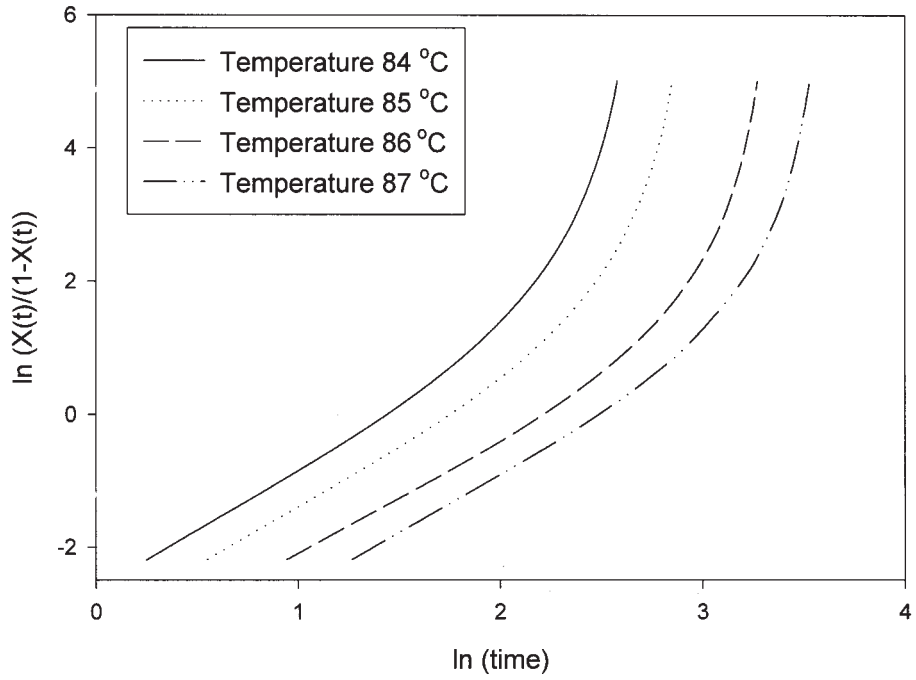

(A)

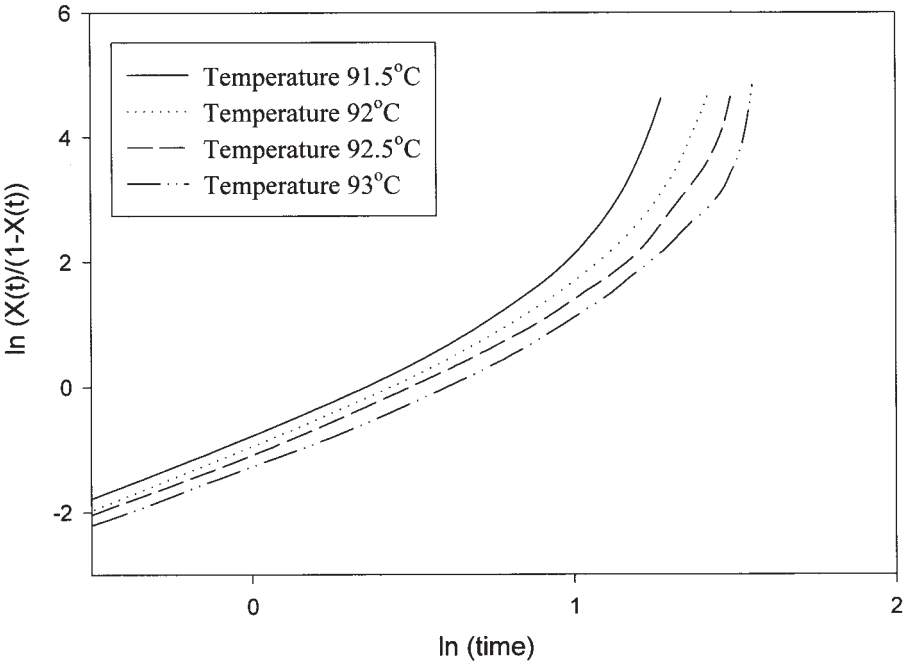

(B)

Figure 6 Tobin analysis from eq. (8) for PEGMA and PEGMA/clay nanocomposites: (A) PEGMA, (B) PEGMA/clay1, (C) PEGMA/clay3, and (D) PEGMA/clay5.

Both Avrami and Tobin crystallization rate constants suggested that the rate of isothermal crystallization increased as T_c decreased and that clay facilitated the crystallization process if present in a small amount, but too much clay slowed down the process.

Malkin analysis

Malkin et al.[55] derived the following equation based on the assumption that the overall crystallization rate equals the summation of the rate at which the degree of crystallinity varies with the emergence of the pri-

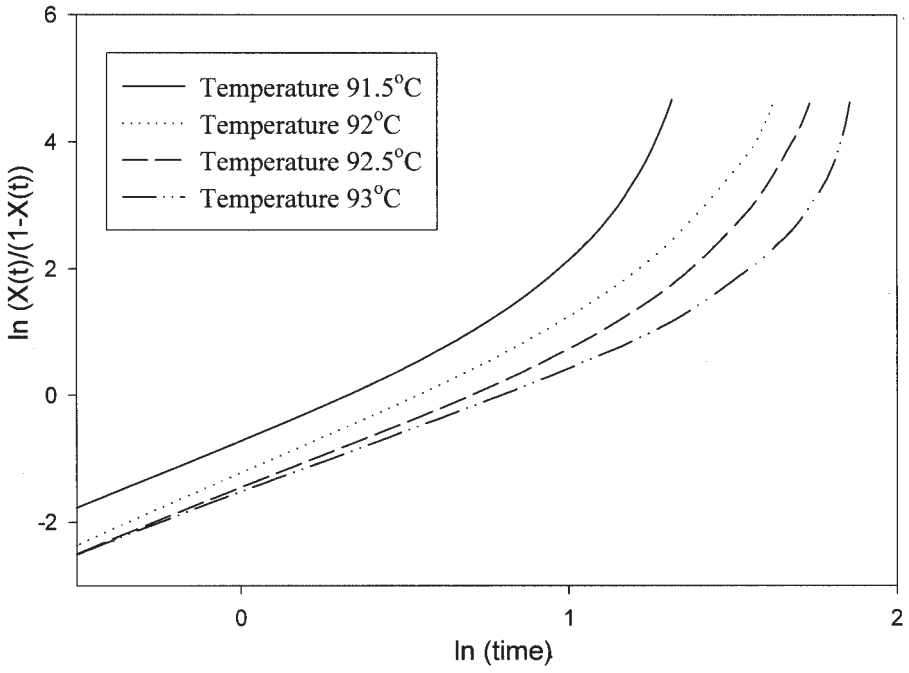

(C)

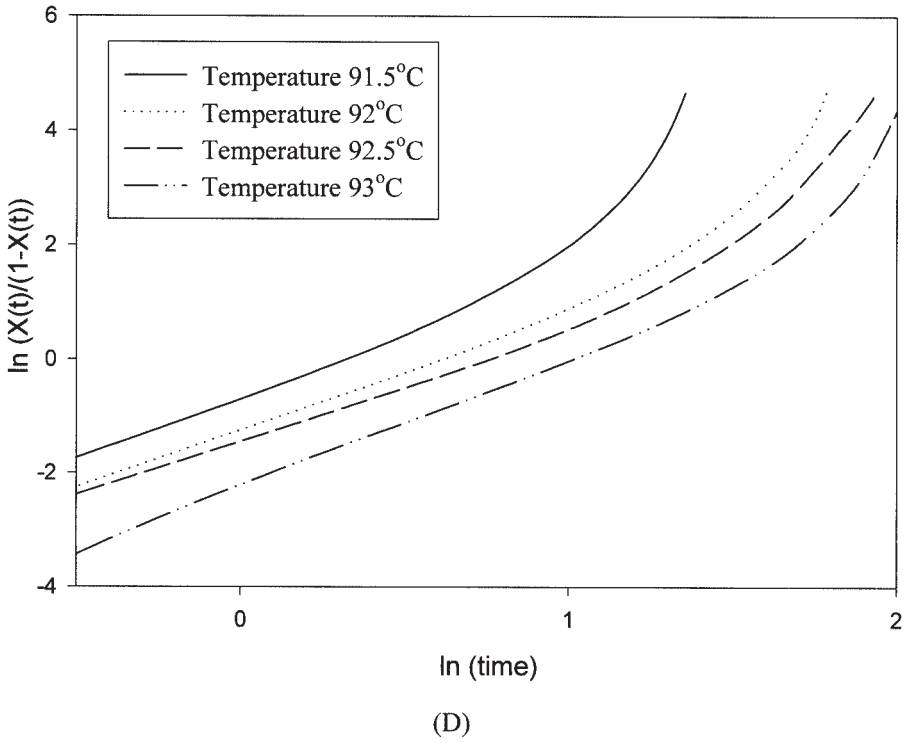

(D)

Figure 6 (*Continued from the previous page*)

mary nuclei and the rate of variation in the degree of crystallinity varies with the crystal growth rate:

$$X(t) = 1 - \frac{C_0 + 1}{C_0 + \exp(C_1 t)} \qquad (10)$$

where C_0 is the Malkin exponent defined as the ratio of the crystal growth rate to the primary nucleation and C_1 is the Malkin crystallization rate constant, which is related to the overall crystallization. C_0 and C_1 were found by the fitting of experi-

TABLE IV
Malkin Kinetic Parameters

Sample	T_c (°C)	C_0	C_1 (min^{-1})	R^2	C_0*	C_1* (min^{-1})
PEGMA	84	4.32	0.4287	0.9988	4.34	0.4499
	85	4.46	0.3185	0.9987	4.22	0.3302
	86	4.23	0.1983	0.9984	3.57	0.2073
	87	4.65	0.1558	0.9984	4.00	0.1519
PEGMA and 1% clay	91.5	8.50	1.6349	0.9988	7.47	1.6439
	92	9.65	1.5911	0.9989	8.82	1.5854
	92.5	7.12	1.3216	0.9987	7.00	1.3423
	93	7.70	1.2217	0.9992	7.00	1.2324
PEGMA and 3% clay	91.5	7.78	1.6153	0.9987	7.47	1.5717
	92	7.36	1.2652	0.9980	8.13	1.2718
	92.5	6.53	1.0411	0.9986	6.41	1.0586
	93	3.97	0.7800	0.9976	5.85	0.8113
PEGMA and 5% clay	91.5	6.59	1.5190	0.9992	6.70	1.5496
	92	4.43	0.9720	0.9982	5.19	1.0081
	92.5	4.38	0.8487	0.9989	4.57	0.8840
	93	6.92	0.7607	0.9979	6.27	0.7839

mental data to eq. (10), and the results are shown in Table IV.

Unlike the Avrami and Tobin models, there is no direct analytical procedure for the determination of the Malkin kinetic parameters.[56] The most important feature for the Malkin model is not its physical meaning but the convenience of its analytical form.[55] From the original article, the Malkin model seems to have a better correlation to the experimental data than the Avrami model in some polymer systems; Figure 5 and the regression coefficient, however, show that the Avrami model provided a slightly better fit than the Malkin model in this study.

Estimated values of C_0 and C_1 can be related to n_a as follows:[55]

$$C_0^* = 4^{n_a} - 4 \tag{11}$$

$$C_1^* = \frac{\ln(4^{n_a} - 2)}{(\ln 2)^{\frac{1}{n_a}}} K_a \tag{12}$$

The estimated Malkin exponent and Malkin crystallization rate constant are shown in Table IV for comparison.

Urbanovici–Segal analysis

Urbanovici and Segal[57] suggested a kinetic equation:

$$X(t) = 1 - [1 + (r - 1)(K_{us}t)^{n_{us}}]^{1/(1-r)} \tag{13}$$

where K_{us} and n_{us} are the Urbanovici–Segal crystallization rate constant and exponent, respectively. When r approaches unity, the Urbanovici–Segal equation reduces to the Avrami model,[53] and this suggests that r is indicative of the deviation of the Urbanovici–Segal equation from the Avrami equation. K_{us} and n_{us} have a physical meaning similar to that of K_a and n_a of the Avrami equation.

The Urbanovici–Segal kinetic equation was also conducted by the fitting of the experimental $X(t)$ data to eq. (13), and the results are shown in Table V. When r was greater than 1, the values of the Urbanovici–Segal kinetic parameters were greater than those of Avrami. When r was 1.12 (in PEGMA/clay3 at 92°C), the difference between n_{us} and n_a was 6.9%, and that between K_{us} and K_a was 4.5%. When r was less than 1, the values of the Urbanovici–Segal kinetic parameters were less than those of Avrami. When r was 0.73 (in neat PEGMA at 86°C), the difference between n_{us} and n_a was −13.5%, and that between K_{us} and K_a was as much as −11.3%.

K_{us} was also estimated from $t_{1/2}$ as follows:

$$K_{us}^* = \left(\frac{0.5^{(1-r)} - 1}{r - 1}\right)^{1/n_{us}} t_{1/2}^{-1} \tag{14}$$

The estimated values of K_{us}^* are listed in Table V. The results of the Urbanovici–Segal analysis showed a crystallization trend similar to those revealed by the Avrami, Tobin, and Malkin models, and the Urbanovici–Segal model provided the best fitting with the highest R^2 value.

Crystallite morphology

Figure 7 shows polarized optical photomicrographs of the neat PEGMA and PEGMA/clay nanocomposites. Spherulites of neat PEGMA [Fig. 7(a)] were larger than those of the PEGMA/clay composites [Fig. 7(b–d)]. The average dimension of the spherulite in the composite decreased dramatically with the addition of

TABLE V
Urbanovici–Segal Kinetic Parameters

Sample	T_c (°C)	n_{us}	r	K_{us} (min^{-1})	R^2	K_{us}* (min^{-1})
PEGMA	84	1.47	0.89	0.1788	0.9998	0.1894
	85	1.43	0.83	0.1279	0.9997	0.1342
	86	1.34	0.73	0.0771	0.9997	0.0781
	87	1.38	0.75	0.0595	0.9997	0.0611
PEGMA and 1% clay	91.5	1.66	0.91	0.5615	0.9998	0.6111
	92	1.79	0.93	0.5269	0.9998	0.5956
	92.5	1.66	0.91	0.4755	0.9997	0.5323
	93	1.68	0.9	0.4292	0.9999	0.4773
PEGMA and 3% clay	91.5	1.71	0.91	0.5595	0.9997	0.6108
	92	1.86	1.12	0.4846	0.9996	0.5509
	92.5	1.64	0.93	0.3873	0.9997	0.4278
	93	1.45	0.89	0.3336	0.9990	0.3540
PEGMA and 5% clay	91.5	1.68	0.92	0.5517	0.9997	0.6001
	92	1.61	1.05	0.4288	0.9996	0.4671
	92.5	1.51	0.95	0.3600	0.9998	0.3853
	93	1.68	0.95	0.2833	0.9997	0.3792

clay, and the spherulites in the nanocomposite were less perfect than those in the neat PEGMA. The polymer spherulite dimension was governed by the number of nuclei formed in a unit of volume at the time of crystallization. The addition of clay resulted in a high nucleus density and smaller spherulites through the impinging effect. The presence of clay also distorted the crystalline phase structure and rendered spherulites less perfect.

CONCLUSIONS

The montmorillonite clay used in this study was easily intercalated via melt blending in a twin-screw extruder with PEGMA to form homogeneous and stable PEGMA/clay nanocomposites. The Avrami, Tobin, Malkin, and Urbanovici–Segal models were used to describe the isothermal crystallization process of neat PEGMA and PEGMA/clay composites. The kinetic analyses of all four models indicated that the addition of clay facilitated the crystallization of PEGMA and that clay could be considered a nucleating agent. When added in greater amounts, however, clay physically hindered the diffusion of molecular chains and retarded the overall crystallization of PEGMA.

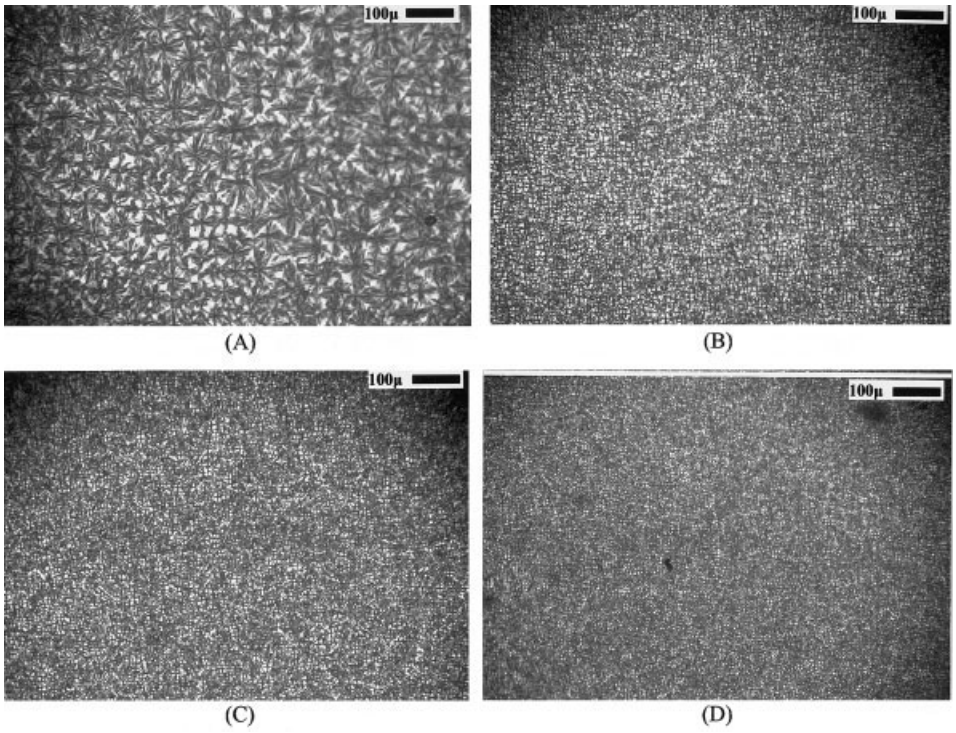

Figure 7 Polarized optical micrographs for (A) PEGMA, (B) PEGMA/clay1, (C) PEGMA/clay3, and (D) PEGMA/clay5.

References

1. Whiteside, G. M.; Mathias, T. P.; Seto, C. T. Science 1991, 254, 1312.
2. Gleiter, H. Adv Mater 1992, 4, 474.
3. Novak, B. Adv Mater 1993, 5, 422.
4. Messersimith, P. B.; Giannelis, E. P. J Polym Sci Part A: Polym Chem 1995, 33, 1047.
5. Usuki, A.; Kawasumi, T.; Kojima, M.; Fukushima, Y.; Okada, A. J Mater Res 1993, 8, 1179.
6. Kojima, Y.; Usuki, A.; Kawasumi, M.; Fukushima, Y.; Okada, A.; Kurauchi, T. J Mater Res 1993, 8, 1185.
7. Yano, K.; Usuki, A.; Okada, A.; Kurauchi, T.; Kamigato, O. J Polym Sci Part A: Polym Chem 1993, 31, 2493.
8. Wang, K. H.; Choi, M. H.; Koo, C. M.; Xu, M.; Chung, I. J.; Jang, M. C.; Choi, S. W.; Song, H. H. J Polym Sci Part B: Poly Phys 2002, 40, 1451.
9. Fukushima, Y.; Okada, A.; Kawasumi, M.; Kurauchi, T.; Kamigaito, O. Clay Miner 1988, 23, 27.
10. Giannelis, E. P. Adv Mater 1996, 8, 29.
11. Wang, M. S.; Pinnavaia, T. J. Chem Mater 1994, 6, 468.
12. Messersmith, P. B.; Giannelis, E. P. Chem Mater 1994, 6, 1719.
13. Vaia, R. A.; Ishii, H.; Giannelis, E. P. Chem Mater 1993, 5, 1694.
14. Vaia, R. A.; Vasudevan, S.; Krawiec, W.; Scanlon, L. G.; Giannelis, E. P. Adv Mater 1995, 7, 154.
15. Kawasumi, M.; Hasegawa, N.; Kato, M.; Usuki, A.; Okada, A. Macromolecules 1997, 30, 6333.
16. Kaempfer, D.; Thomann, R.; Mohlhaupt, R. Polymer 2002, 43, 2909.
17. Reichert, P.; Nitz, H.; Klinke, S.; Brandsch, R.; Thomann, R.; Mulhaupt, R. Macromol Mater Eng 2000, 275, 8.
18. Zanetti, A. U.; Camino, G.; Canavese, D.; Morgan, A. B.; Lamelas, F. J.; Wilkie, C. A. Chem Mater 2002, 14, 189.
19. Kawasumi, M.; Hasegawa, N.; Kato, M.; Usuki, A.; Okada, A. Macromolecules 1997, 30, 6333.
20. Hasegawa, N.; Kawasumi, M.; Kato, M.; Usuki, A.; Okada, A. J Appl Polym Sci 1998, 67, 87.
21. Adams, T.; Oliver, W.; Martina, M. P.; Manfred, P. H.; Bernhard, S. Polym Degrad Stab 2003, 82, 133.
22. Kaempfer, D.; Thomann, R.; Mohlhaupt, R. Polymer 2002, 43, 2909.
23. Reichert, P.; Nitz, H.; Klinke, S.; Brandsch, R.; Thomann, R.; Mulhaupt, R. Macromol Mater Eng 2000, 275, 8.
24. Zanetti, A. U.; Camino, G.; Canavese, D.; Morgan, A. B.; Lamelas, F. J.; Wilkie, C. A. Chem Mater 2002, 14, 189.
25. Liang, G.; Xu, J.; Bao, S.; Xu, W. J Appl Polym Sci 2004, 91, 3974.
26. Hoffman, J. D.; Weeks, J. J. J Res Natl Bur Stand Sect A 1962, 66, 13.
27. Lee, S. W.; Lee, B.; Ree, M. Macromol Chem Phys 2000, 201, 453.
28. Kuo, S. W.; Huang, W. J.; Huang, S. B.; Kao, H. C.; Chang, F. C. Polymer 2003, 44, 7709.
29. Kolmogorov, A. N.; Akad, I. Nauk USSR Ser Mater 1937, 1, 355.
30. Johnson, W. A.; Mehl, K. F. Trans Am Inst Min Met Eng 1939, 135, 416.
31. Avrami, M. J Chem Phys 1939, 7, 1103.
32. Avrami, M. J Chem Phys 1940, 8, 212.
33. Avrami, M. J Chem Phys 1941, 9, 177.
34. Evans, U. R. Trans Faraday Soc 1945, 41, 365.
35. Ding, Z. J.; Spruiell, E. J Polym Sci Part B: Polym Phys 1997, 35, 1077.
36. Long, Y.; Shanks, R. A.; Stachurski, Z. H. Prog Polym Sci 1995, 20, 651.
37. Siyang, L.; Yingning, Y.; Yi, C.; Hongfang, Z.; Zhishen, M. J Appl Polym Sci 1998, 70, 2371.
38. Liu, S.; Yu, Y.; Yi, C.; Zang, H.; Mo, Z. J Appl Polym Sci 1998, 70, 2371.
39. Supaphol, P.; Spruiell, J. E. Polymer 2001, 42, 699.
40. Wunderlich, B. Macromolecular Physics; Academic: New York, 1976; Vol. 2.
41. Supaphol, P. Thermochim Acta 2001, 370, 37.
42. Bicerano, J. J Macromol Sci Polym Rev 1998, 38, 391.
43. Fatou, J. G. Makromol Chem 1984, 7, 131.
44. Zhang, G.; Yan, D. J Appl Polym Sci 2003, 88, 2181.
45. Ma, C. C.; Kuo, C. T.; Kuan, H. C.; Chiang, C. L. J Appl Polym Sci 2003, 88, 1686.
46. Jimenez, C. G.; Ogata, N.; Kawai, H.; Ogihara, T. J Appl Polym Sci 1997, 64, 2211.
47. Tobin, M. C. J Polym Sci Polym Phys Ed 1974, 12, 399.
48. Tobin, M. C. J Polym Sci Polym Phys Ed 1976, 14, 2253.
49. Tobin, M. C. J Polym Sci Polym Phys Ed 1977, 15, 2269.
50. Supaphol, P. J Appl Polym Sci 2000, 78, 338.
51. Qiu, Z.; Ikehara, T.; Nishi, T. Polymer 2003, 44, 5429.
52. Ravindranath, K.; Jog, J. P. J Appl Polym Sci 1993, 49, 1395.
53. Cruz-Pinto, J. J. C.; Martins, J. A.; Oliveira, M. J. Colloid Polym Sci 1994, 272, 1.
54. Supaphol, P.; Spruiell, J. E. J Macromol Sci Phys 2000, 39, 257.
55. Malkin, A. Y.; Beghishev, V. P.; Keapin, I. A.; Bolgov, S. A. Polym Eng Sci 1984, 24, 1396.
56. Dangseeyun, N.; Srimoaon, P.; Supaphol, P.; Nithitanakul, M. Thermochim Acta 2001, 370, 37.
57. Urbanovici, E.; Segal, E. Thermochim Acta 1990, 171, 87.